Quantitative coherent scattering spectra in apertureless terahertz pulse near-field microscopes

Article *in* Applied Physics Letters · July 2012

DOI: 10.1063/1.4733475

AIP | Applied Physics Letters

Quantitative coherent scattering spectra in apertureless terahertz pulse near-field microscopes

Kiwon Moon, Youngwoong Do, Meehyun Lim, Gyuseok Lee, Hyeona Kang et al.

Citation: Appl. Phys. Lett. **101**, 011109 (2012); doi: 10.1063/1.4733475
View online: http://dx.doi.org/10.1063/1.4733475
View Table of Contents: http://apl.aip.org/resource/1/APPLAB/v101/i1
Published by the American Institute of Physics.

Quantitative coherent scattering spectra in apertureless terahertz pulse near-field microscopes

Kiwon Moon, Youngwoong Do, Meehyun Lim, Gyuseok Lee, Hyeona Kang, Kee-Su Park, and Haewook Han[a)]
Department of Electrical and Computer Engineering, POSTECH, Pohang, Kyungbuk 790-784, South Korea

(Received 19 March 2012; accepted 18 June 2012; published online 5 July 2012)

We present quantitative coherent measurements of scattering pulses and spectra in terahertz apertureless near-field microscopes. Broadband near-field image contrasts for both amplitude and phase spectra are measured directly from time-domain scattering signals with an unprecedentedly high single-scan signal-to-noise ratio (~48 dB), with approach curves for both short (<200 nm) and long (up to 82 μm) ranges. By using the line dipole image method, we obtain quantitative broadband THz imaging contrasts with nanoscale resolution. © *2012 American Institute of Physics*. [http://dx.doi.org/10.1063/1.4733475]

Scanning near-field microscopy has long been recognized as an important method for studying semiconductor nanostructures and biomolecular systems. In the IR and mid-IR regions, scattering-type apertureless scanning near field optical microscopes (s-SNOMs) have been developed,[1–6] where coherent optical pulses[4,5] and thermal emission[6] were used for broadband measurements, and also the phase spectra were obtained by using interferometric techniques.[2–6] In addition to these instrumental improvements, theoretical approaches such as the point dipole image method (PDIM)[7] and finite dipole image method (FDIM)[8] were also developed for quantitative analyses of near-field measurements.

Meanwhile, considerable efforts have been made to develop near-field imaging techniques in the terahertz (THz) region.[9–23] Most of these THz near-field microscopes have been based on THz time-domain spectroscopy (THz-TDS).[24] In principle, these THz pulse s-SNOMs should be able to provide both amplitude and phase spectra of the near-field scattering THz pulses for quantitative THz near-field microscopy in which the local optical properties such as complex permittivity and conductivity are determined from the THz near-field scattering pulses. However, the lack of a high-powered coherent broadband THz source[25] and accurate theoretical models has hampered the realization of quantitative nanoscale imaging contrast in the THz region for a long time. Recently, the peak amplitudes of near-field scattering signals in THz pulse s-SNOMs have been measured on dielectric and metallic substrates; in addition, a self-consistent line dipole image method (LDIM) based on an exact quasi-electrostatic image theory has been developed for the analysis of THz s-SNOMs, in which the measured approach curves are in good agreement with LDIM calculations.[21,22]

However, the direct broadband measurements of both amplitude and phase spectra for THz pulse s-SNOMs have not yet been demonstrated. For instance, in Ref. 20, THz scattering pulses were measured in time-domain only for a gold surface, but quantitative spectra and image contrast were not obtained. In Ref. 23, a high-power monochromatic continuous-wave THz laser was used for the nano-scale near-field imaging, but neither broadband spectra nor quantitative image contrast was obtained as well. In this work, we report on the quantitative broadband scattering signals and imaging contrasts of a THz-pulse s-SNOM in both amplitude and phase spectra, directly measured from THz time-domain scattering pulses, with an unprecedented signal-to-noise ratio (SNR). The THz near-field imaging contrast was quantitatively analyzed by near-field calculations based on the self-consistent LDIM.

The THz pulse s-SNOM system is based on an atomic force microscope (AFM). We used a high-resistivity (>10 kΩ cm) float-zone (FZ) Si wafer partially coated by a 30-nm thick gold film. The THz pulse was generated by an InAs wafer pumped by a Ti:sapphire laser with a center wavelength of 800 nm, a pulse width of 10 fs, and a repetition rate of 100 MHz. The incident THz pulse (E_{in}) was p-polarized and focused on a tungsten AFM tip fabricated by an electro-chemical etching method. The forward-scattering THz pulse (E_s) from the tip apex was then detected by a photoconductive antenna fabricated on low-temperature-grown GaAs in the far-field region, where the incident and scattering angles were 60°. The entire THz s-SNOM system was enclosed in a chamber and continuously purged with dry air to eliminate the THz absorption by water vapor in air.

The AFM tip was modulated by using a quartz tuning fork driven at a mechanical resonance frequency (Ω). The tip-to-sample distance was given by $d(t) = d_0 + a\cos\Omega t$, where the average distance (d_0) and dithering amplitude (a) were precisely controlled by a proportional-integral-derivative (PID) controller with t as the time coordinate for the sinusoidal tip oscillation. The scattering signal has a strong nonlinear dependence on the tip-to-sample distance; hence, E_s can be expressed by the sum of harmonics E_m at mΩ with a fixed position on a delay line.[7,8,21,22] In the THz s-SNOM, E_s contains local optical information of the sample surface, and the strong light localization at the tip apex provides nanoscale resolution.[26] Given that E_m is much smaller than the specularly reflected, background signal E_0, we used lock-in demodulation at mΩ to extract E_m by suppressing E_0 and other harmonics. In visible or IR s-SNOMs, E_2 and E_3 have usually been preferred to E_1[3–8,28] because higher harmonics are known to be more effective in suppressing background

a)Electronic mail: hhan@postech.ac.kr.

artifacts generated from signal mixing at the optical power detector, along with interferometric techniques.[2,3,27–30] There was however no signal mixing in the THz-pulse s-SNOM system because the photoconductive antenna detects the instantaneous electric fields of THz pulses rather than the power. This means that THz-pulse s-SNOMs can also measure the phase contrast without the interferometric technique used in IR s-SNOMs.[2,3]

The time-domain scattering signals and their spectra of THz pulses for E_{in}, E_1(Au), and E_1(Si) are shown in Fig. 1, where the signals for Au and Si show a time delay (~0.3 ps) relative to the reference signal. This is strong evidence that the near-field interaction between the probe and sample surface cause the time delays. The demodulation frequencies for the lock-in detection were 2 kHz (optical chopper) and mΩ ($\Omega = 31$ kHz for the quartz tuning fork, $m = 1$, 2) for measurements of the excitation and scattering fields, respectively. The peak amplitudes of E_1(Au) and E_1(Si) were ~200 and 800 times smaller, respectively, than the amplitude of the excitation pulse. The relative spectral amplitudes were 10^{-2} to 10^{-3} which is in reasonable agreement with those in Ref. 18. The field SNR of E_1(Au) was as high as ~250, corresponding to ~48 dB, for a single scan without averaging. The lock-in integration and single scan times were 300 ms and 72 s, respectively. This is the highest SNR ever reported in a THz pulse s-SNOM system.

The measured and calculated contrasts of the amplitude and phase spectra given by E_1(Si)/E_1(Au) are shown in Fig. 2. The amplitude ratio and phase difference between E_1(Au)/E_{in} and E_1(Si)/E_{in} were nearly constant over a broad spectral range of up to 2 THz while the normalized amplitude spectra showed high-frequency enhancement. The LDIM calculation (dashed lines) shows that the amplitude contrast is ~0.25. In addition, the phase contrasts are as small as 0.5–2.8 mrad and nearly frequency-independent as expected. This is simply because at THz frequencies, the tungsten probe is a good conductor and FZ-Si is a nearly dispersion-free and lossless dielectric material. Although the measurements are in reasonably good agreement with the calculations, there are small discrepancies. This is because although the LDIM is self-consistent within the framework of the sphere model, it is an approximate model. We expect that these small discrepancies and the high-frequency enhancement can be explained by

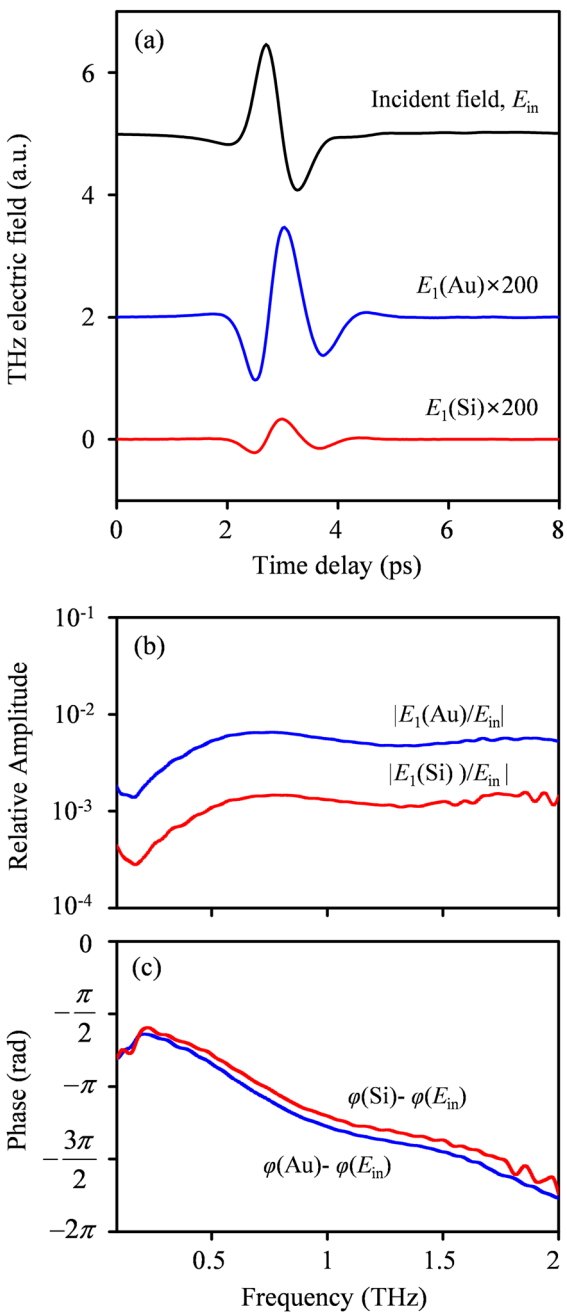

FIG. 1. Measured THz incident and scattering pulses on gold and FZ-Si surfaces. (a) Time-domain signals, (b) normalized amplitude spectra, and (c) normalized phase spectra.

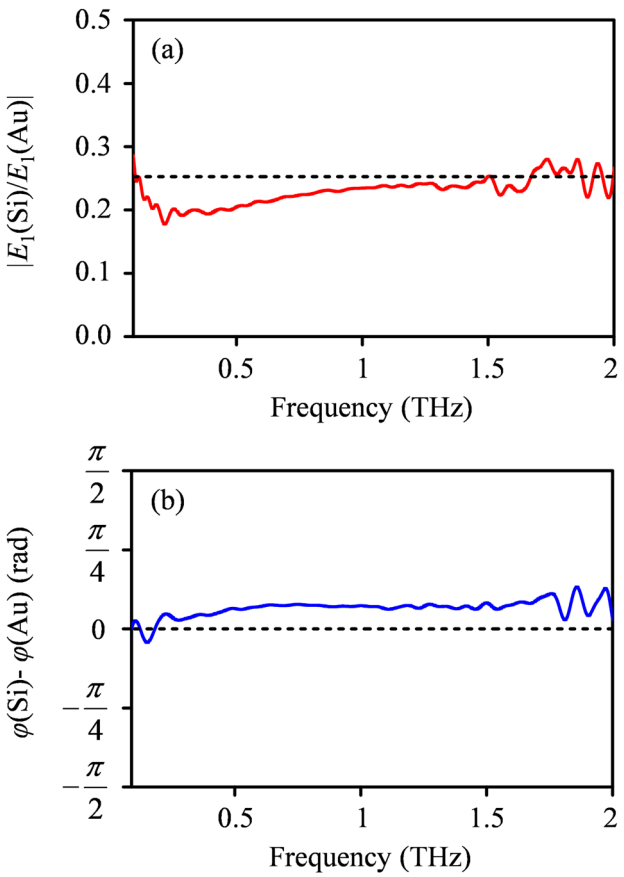

FIG. 2. Measured (solid lines) and calculated (dotted lines) contrasts between E_1(Au) and E_1(Si): (a) amplitude contrast and (b) phase contrast.

using the full antenna model in our calculations. It should be noted that the quantitative measurement of these spectrally featureless contrasts (both amplitude and phase) is of great importance since it can serve as a calibration test for samples with characteristic spectral features.

Shown in Fig. 3(a) are the short-range approach curves of E_1 and E_2 at Au and Si surfaces. The mechanical delay line was fixed at the positive peak position of the scattering THz pulse during measurements. All the approach curves were measured at position a few millimeters away from the edge of the gold film to avoid potential fringing field effects. The closed circles in Fig. 3(a) represent experimental results normalized to the maximum of the E_1(Au), which is the largest scattering signal. As the minimum tip-to-sample distance decreases, the approach curves of E_2 show a steeper increase than those of E_1, which is consistent with previous results in visible and IR s-SNOMs.[2,3,7] This is convincing experimental evidence for the near-field interaction between the tip apex and the sample surface. Moreover, no undulation was observed in the approach curves, which can be expected from the fact that the tip-to-sample distance is much smaller than the THz wavelength. In comparison, Fig. 3(b) shows the long-range approach curve of E_1 at an Au surface, measured up to $d_0 = 82\,\mu$m. The scattering signal E_1 decays extremely fast in a short range ($<2.2\,\mu$m) and is further reduced to 0.014 at $d_0 = 82\,\mu$m. This indicates that the background contribution still exists but is very small in our THz pulse s-SNOM.

Most previous analytical models used for the theoretical calculation of approach curves were based on the simple PDIM where the probe tip was replaced with a polarizable sphere on semi-infinite metallic or dielectric substrates.[1–4,7,21,22] However, the PDIM is not self-consistent,[1–4,7] because the quasi-electrostatic boundary conditions are inadequately satisfied at the surfaces of the probe spheres and substrates. In this work, we used the LDIM in which all exact boundary conditions are

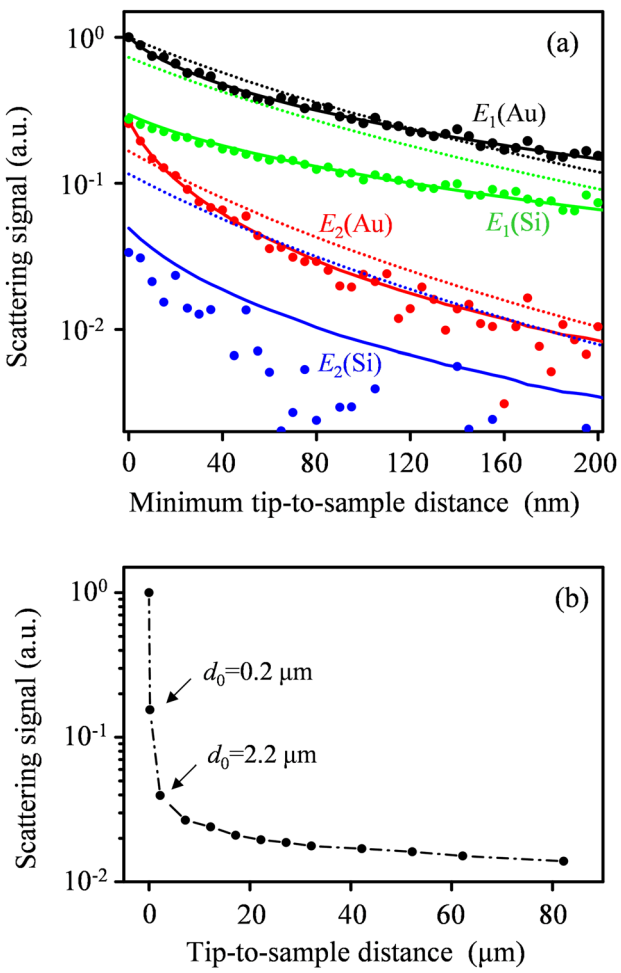

FIG. 3. Approach curves of a THz pulse SNOM: (a) short-range E_1 and E_2 on gold and FZ-Si surfaces. The dots and solid lines in (a) represent experiments and calculations by the LDIM, respectively. The black, green, red, and blue closed circles (experiments) and lines (theory) are for E_1(Au), E_1(Si), E_2(Au), and E_2(Si), respectively. (b) Long-range E_1 on a gold surface where the approach curve was measured up to $d_0 = 82\,\mu$m.

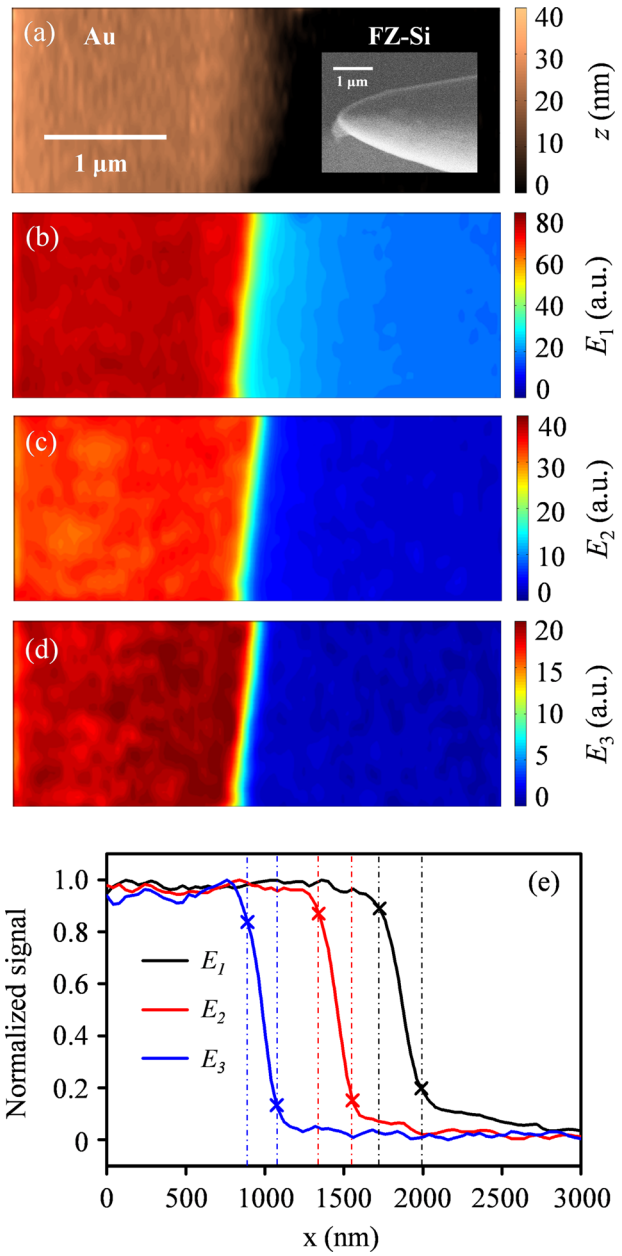

FIG. 4. Images of a partially Au-coated FZ-Si sample. (a) AFM topography and (b)-(d) THz near field images of E_1, E_2, and E_3. (e) Normalized scan profiles for E_1, E_2, and E_3. The 90%–10% resolutions are 265 nm, 215 nm, and 185 nm for E_1, E_2, and E_3 images, respectively. The inset in (a) shows the scanning electron microscope image of the tip apex.

satisfied by a regenerative iteration processes.[21,22] The total induced dipole moment in the probe and image spheres was calculated by the LDIM for a sinusoidal motion of the probe sphere, from which the harmonic components of the THz scattering fields were calculated in the far-field region.

As can be seen in Fig. 3(a), the approach curves calculated by the LDIM (solid lines) were in good agreement with the experimental curves, whereas the PDIM calculations (dotted lines) showed significant deviation from the experiments. For the calculation of the approach curves, we used a dithering amplitude of $a = 45$ nm, which was precisely controlled by a PID controller. For the best-fit curves for the first and second harmonic components, the effective radii of the probe tip estimated from the LDIM and PDIM were 1100 nm and 300 nm, respectively. For the frequency-dependent complex dielectric constants of gold and tungsten, we used the Drude model where the plasma (damping) frequencies of gold and tungsten were 2184 THz (1551 THz) and 6.45 THz (14.61 THz), respectively.[31] For the FZ-Si wafer, we used a frequency-independent lossless refractive index of 3.42.[32]

Figure 4 shows the AFM topography and THz-pulse near-field images of E_1, E_2, and E_3 measured with a smaller tip radius of ~280 nm for higher resolution. The dimensions of the images were $4 \times 1.4\ \mu m^2$ (100×20 pixels). Normalized line scans across the edge of the gold film for E_1, E_2, and E_3 are shown in Fig. 4(e). The 90%–10% spatial resolutions were measured to be 265, 215, and 185 nm for the E_1, E_2, and E_3 images, respectively. This resolution enhancement for higher harmonics can also be predicted from the approach curves, consistent with previous studies in IR s-SNOMs.[2,3,7] Moreover, there is no sign of background artifacts even in the E_1 image.

In summary, we have constructed a THz s-SNOM system that is capable of quantitative coherent imaging contrast for both amplitude and phase. Approach curves and near-field imaging for Au/Si substrates were obtained directly from time-domain THz scattering signals with a high SNR of ~250 for a single scan without averaging. For the THz near-field analysis, we used LDIM calculations, which were in good agreement with experiments. We believe that this is an important step toward quantitative THz spectroscopic nanoscale imaging and may find many applications for the study of semiconductor nanostructures and biomolecular systems.

This work was supported by the Basic Science Research Program (2009-0093429), the Priority Research Centers Program through the National Research Foundation of Korea (NRF) funded by the Ministry of Education, Science and Technology (2011-0031405), the Brain Korea 21 Project in 2012, and the IT Consilience Creative Program (C1515-1121-0003).

[1] B. Knoll and F. Keilmann, Nature (London) **399**, 134–137 (1999).
[2] R. Hillenbrand and F. Keilmann, Phys. Rev. Lett. **85**, 3029–3032 (2000).
[3] R. Hillenbrand, B. Knoll, and F. Keilmann, J. Microsc. **202**, 77–83 (2001).
[4] M. Brehm, A. Schliesser, and F. Keilmann, Opt. Express **23**, 11222–11233 (2006).
[5] S. Amarie and F. Keilmann, Phys. Rev. B **83**, 045404 (2011).
[6] F. Huth, M. Schnell, J. Wittborn, N. Ocelic, and R. Hillenbrand, Nat. Mater. **10**, 352–356 (2011).
[7] B. Knoll and F. Keilmann, Opt. Commun. **182**, 321–328 (2000).
[8] A. Cvitkovic, N. Ocelic, and R. Hillenbrand, Opt. Express **15**, 8550–8565 (2007).
[9] S. Hunsche, M. Koch, I. Brener, and M. C. Nuss, Opt. Commun. **150**, 22–26 (1998).
[10] Q. Chen and X.-C. Zhang, IEEE J. Sel. Top. Quantum Electron. **7**, 608–614 (2001).
[11] N. C. J. van der Valk and P. C. M. Planken, Appl. Phys. Lett. **81**, 1558–1560 (2002).
[12] A. Bitzer and M. Walther, Appl. Phys. Lett. **92**, 231101 (2008).
[13] J. R. Knab, A. J. L. Adam, R. Chakkittakandy, and P. C. M. Planken, Appl. Phys. Lett. **97**, 031115 (2010).
[14] H.-T. Chen, R. Kersting, and G. C. Cho, Appl. Phys. Lett. **83**, 3009–3011 (2003).
[15] H.-T. Chen, S. Kraatz, G. C. Cho, and R. Kersting, Phys. Rev. Lett. **93**, 267401 (2004).
[16] K. Wang, D. M. Mittleman, N. C. J. van der Valk, and P. C. M. Planken, Appl. Phys. Lett. **85**, 2715–2717 (2004).
[17] H. Park, J. Kim, and H. Han, in *35th Workshop: Physics and Technology of THz Photonics*, Erice, Italy, 20–26 July 2005.
[18] H.-G. von Ribbeck, M. Brehm, D. W. van der Weide, S. Winnerl, O. Drachenko, M. Helm, and F. Keilmann, Opt. Express **16**, 3430–3438 (2008).
[19] U. Schade, K. Holldack, P. Kuske, and G. Wüstefeld, Appl. Phys. Lett. **84**, 1422–1424 (2004).
[20] V. N. Trukhin, A. V. Andrianov, V. A. Bykov, A. O. Golubok, N. N. Zinov'ev, L. L. Samoilov, I. D. Sapozhnikov, A. V. Trukhin, and M. L. Fel'shtyn, JETP Lett. **93**, 119–123 (2011).
[21] K. Moon, E. Jung, M. Lim, Y. Do, and H. Han, IEEE Trans. THz Sci. Technol. **1**, 164–168 (2011).
[22] K. Moon, E. Jung, M. Lim, Y. Do, and H. Han, Opt. Express **19**, 11539–11544 (2011).
[23] A. J. Huber, F. Keilmann, J. Wittborn, J. Aizpurua, and R. Hillenbrand, Nano Lett. **8**, 3766–3770 (2008).
[24] B. Ferguson and X. C. Zhang, Nat. Mater. **1**, 26–33 (2002).
[25] M. L. Smith, R. Mendis, R. E. M. Vickers, and R. A. Lewis, J. Appl. Phys. **105**, 063109 (2009).
[26] L. Novotny, R. X. Bian, and X. S. Xie, Phys. Rev. Lett. **79**, 645–648 (1997).
[27] B. Hecht, H. Bielefeldt, Y. Inouye, D. W. Pohl, and L. Novotny, J. Appl. Phys. **81**, 2492–2498 (1997).
[28] M. Labardi, S. Patanè, and M. Allegrini, Appl. Phys. Lett. **77**, 621–623 (2000).
[29] P. G. Gucciardi and M. Colocci, Appl. Phys. Lett. **79**, 1543–1545 (2001).
[30] P. G. Gucciardi, G. Bachelier, M. Allegrini, J. Ahn, M. Hong, S. Chang, W. Jhe, S.-C. Hong, and S. H. Baek, J. Appl. Phys. **101**, 064303 (2007).
[31] M. A. Ordal, R. J. Bell, R. W. Alexander, Jr., L. L. Long, and M. R. Querry, Appl. Opt. **24**, 4493–4499 (1985).
[32] D. Grischkowsky, S. Keiding, M. van Exter, and Ch. Fattinger, J. Opt. Soc. Am. B **7**, 2006–2015 (1990).